

Global Biogeochemical Cycles

RESEARCH ARTICLE

10.1029/2019GB006368

Key Points:

- Progress of ocean acidification in the western tropical Pacific Warm Pool was identified using the data of oceanic CO₂ measurements
- The rate of oceanic CO₂ increase here was ~20% lower than that expected from the growth rate of the mixing ratio of CO₂ in the atmosphere
- Intergyre exchange of anthropogenic CO₂ within the thermocline predominantly controls the rate of acidification in this region

Supporting Information:

- Supporting Information S1

Correspondence to:

M. Ishii,
mishii@mri-jma.go.jp

Citation:













Ishii, M., Rodgers, K. B., Inoue, H. Y., Toyama, K., Sasano, D., Kosugi, N., et al. (2020). Ocean acidification from below in the tropical Pacific. *Global Biogeochemical Cycles*, 34, e2019GB006368. <https://doi.org/10.1029/2019GB006368>

Received 16 JUL 2019

Accepted 16 JUL 2020

Accepted article online 27 JUL 2020

Ocean Acidification From Below in the Tropical Pacific

Masao Ishii¹ , Keith B. Rodgers^{2,3} , Hisayuki Y. Inoue⁴ , Katsuya Toyama¹ , Daisuke Sasano^{1,5} , Naohiro Kosugi¹ , Hisashi Ono¹ , Kazutaka Enyo⁵, Toshiya Nakano^{5,6} , Daniele Iudicone⁷ , Bruno Blanke⁸ , Olivier Aumont⁹ , and Richard A. Feely¹⁰ 

¹Meteorological Research Institute, Japan Meteorological Agency, Tsukuba, Japan, ²Center for Climate Physics, Institute for Basic Science, Busan, South Korea, ³Pusan National University, Busan, South Korea, ⁴Graduate School of Environmental Earth Sciences, Hokkaido University, Sapporo, Japan, ⁵Global Environment and Marine Department, Japan Meteorological Agency, Tokyo, Japan, ⁶Nagasaki Local Meteorological Office, Nagasaki, Japan, ⁷Department of Integrated Marine Ecology, Stazione Zoologica Anton Dohrn, Naples, Italy, ⁸Laboratoire d'Océanographie Physique et Spatiale, Institut Universitaire Européen de la Mer, Brest, France, ⁹Laboratoire d'Océanographie et du Climat: Expérimentations et Approches Numériques, Sorbonne Université-CNRS-IRD-MNHN, Paris, France, ¹⁰Pacific Marine Environmental Laboratory, National Oceanic and Atmospheric Administration, Seattle, WA, USA

Abstract Identifying ocean acidification and its controlling mechanisms is an important priority within the broader question of understanding how sustained anthropogenic CO₂ emissions are harming the health of the ocean. Through extensive analysis of observational data products for ocean inorganic carbon, here we quantify the rate at which acidification is proceeding in the western tropical Pacific Warm Pool, revealing $-0.0013 \pm 0.0001 \text{ year}^{-1}$ for pH and $-0.0083 \pm 0.0007 \text{ year}^{-1}$ for the saturation index of aragonite for the years 1985–2016. However, the mean rate of total dissolved inorganic carbon increase ($+0.81 \pm 0.06 \mu\text{mol} \cdot \text{kg}^{-1} \cdot \text{year}^{-1}$) sustaining acidification was ~20% slower than what would be expected if it were simply controlled by the rate of atmospheric CO₂ increase and transmitted through local air-sea CO₂ equilibration. Joint Lagrangian and Eulerian model diagnostics indicate that the acidification of the Warm Pool occurs primarily through the anthropogenic CO₂ that invades the ocean in the extra-tropics is transported to the tropics through the thermocline shallow overturning circulation and then re-emerges into surface waters within the tropics through the Equatorial Undercurrent from below. An interior residence time of several years to decades, acting in conjunction with the accelerating CO₂ growth in the atmosphere, can be expected to contribute to modulating the rate of Warm Pool acidification.

1. Introduction

The western tropical Pacific is a realm of rich marine biodiversity that accommodates a highly diverse range of coral reef habitats (WorldFish, 2019; Figure 1a). It contains 75% of all known coral species and more than 3,000 species of fish and supports the livelihood of more than 110 million people for whom the associated marine ecosystems provide food, income, and safety through their sustained ecosystem services (Burke et al., 2011). However, the region has been degraded by multiple adverse human activities including overfishing, habitat destruction, and land-sourced pollution (Burke et al., 2012; Roberts et al., 2002). Importantly, coral reef habitats are also thought to have been under increasing stress due to ocean acidification (Hoegh-Guldberg et al., 2007; Kleypas et al., 1999; Langdon et al., 2003; Pandolfi et al., 2011), that is, the increase of hydrogen ion concentration (reduction of pH) and decrease of the saturation level of calcium carbonate minerals in seawater over an extended period of time due to the excess CO₂ uptake from the atmosphere. Together with global warming and associated trends toward sea-level rise and episodic bleaching events, ocean acidification has been driven by increasing CO₂ emissions associated with human activities. Even if anthropogenic CO₂ emissions are substantially reduced over the coming decades, the trend toward acidification is expected to continue to pose risks for calcifying organisms such as corals and mollusks that show greater sensitivity of their growth to ocean acidification (Gattuso et al., 2015). This will have serious large-scale consequences for marine ecosystems and undermine shoreline protection from storm damage and erosion (Albright et al., 2018). The resulting socio-economic impacts anticipated in and around the western tropical Pacific motivate a quantification and attribution of the evolution of ocean acidification in recent decades over this region.

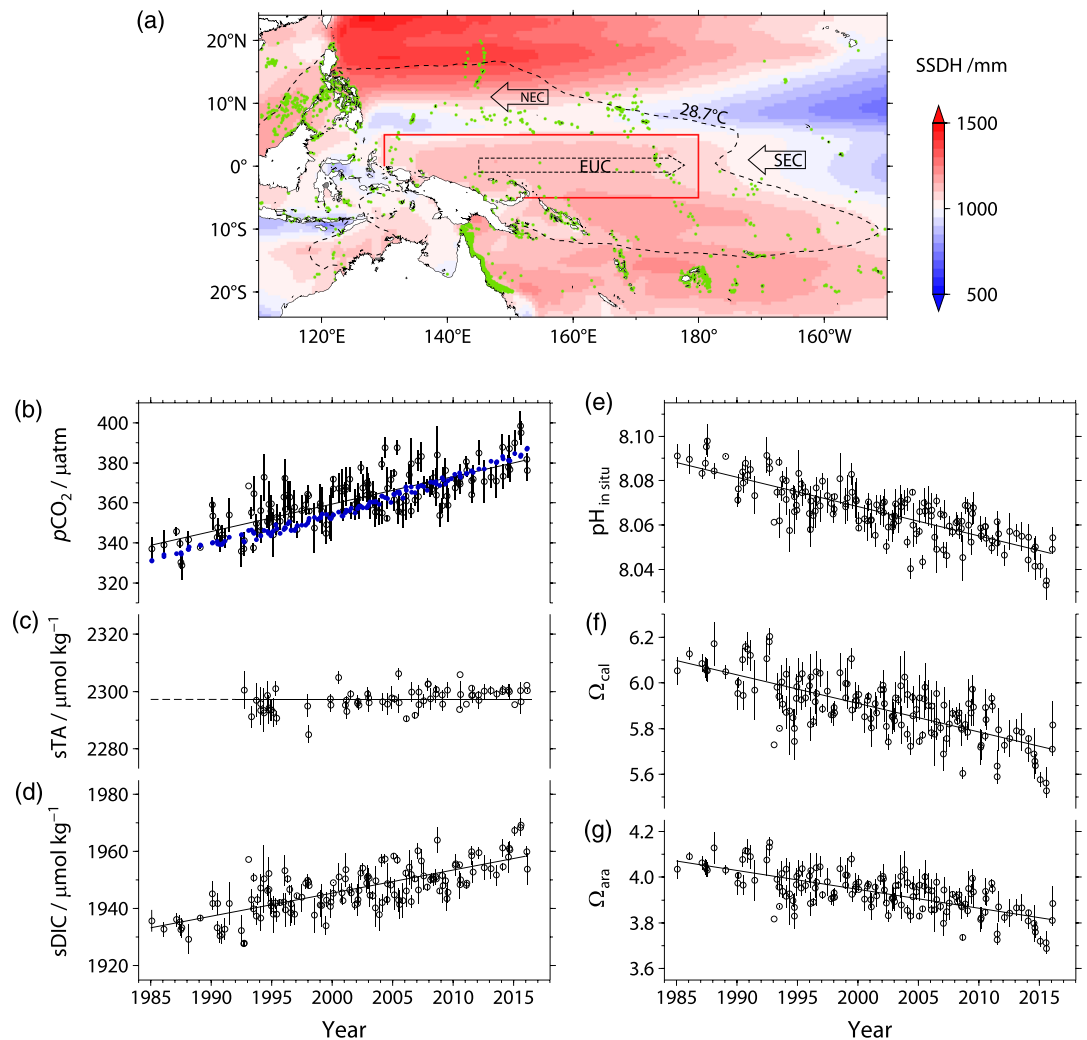


Figure 1. Multidecadal trends toward increasing CO₂ and acidification in the surface layer of the western tropical Pacific Warm Pool. (a) Schematic view of the western tropical Pacific showing the distribution of coral reefs (green plots; WorldFish, 2019). Superposed also on the map are the mean sea surface dynamic height (SSDH; color), the outcrops of the 28.7 °C isotherm at the surface (broken line) for the years 2011–2015 (Japan Meteorological Agency, <https://ds.data.jma.go.jp/gmd/goos/data/rtrdb/jma-pro.html>), and major surface and subsurface currents including the North Equatorial Current (NEC), the South Equatorial Current (SEC), and the Equatorial Undercurrent (EUC; double-dashed arrow). Shown with a red rectangle is the area of observational data analysis evaluated for ocean acidification in this work (130°E–180°, 5°S–5°N). Mean values (open circles) and standard deviations (vertical bars) for each month over the Warm Pool ($T > 28.7$ °C and $S < 34.7$) and their linear trends for 1985–2016 are shown for (b) $p\text{CO}_2\text{sw}$ (black), (c) salinity-normalized ($S = 35$) total alkalinity (sTA), (d) salinity-normalized DIC (sDIC), (e) pH at in situ temperature and salinity, (f) saturation indices of calcium carbonate minerals calcite (Ω_{cal}), and (g) aragonite (Ω_{ara}). Also shown in (b) are the data for $p\text{CO}_2\text{air}$ (blue) measured during the same cruises as those of $p\text{CO}_2\text{sw}$ measurements.

Measurements of the partial pressure of CO₂ in surface seawater ($p\text{CO}_2\text{sw}$) and in the atmosphere ($p\text{CO}_2\text{air}$) have been frequently made in the western tropical Pacific since the mid-1980s. In the mid-1990s to late 2000s, these data revealed a trend toward increasing $p\text{CO}_2\text{sw}$ with the rate having varied over the period of analysis (Feely et al., 1999, 2006; Inoue et al., 1995; Ishii et al., 2009, 2014; Takahashi et al., 2003). More recently, international efforts toward data synthesis and quality control have begun for $p\text{CO}_2\text{sw}$ in the surface layer (Bakker et al., 2016; Pfeil et al., 2013) and other inorganic carbon variables such as total dissolved inorganic carbon (DIC) and total alkalinity (TA) in the surface layer and in the ocean interior (Key et al., 2004; Olsen et al., 2016; Suzuki et al., 2013; Tanhua et al., 2010). Such efforts have enabled continuing integration of data from multiple sources and platforms, thereby providing an account of changes in the

oceanic CO₂ chemistry for both surface and ocean interior waters for a prolonged period extending over the past three decades in a large part of the global oceans as well as in the western tropical Pacific. In addition, the development of Lagrangian diagnostic tools with forward ocean models (e.g., Blanke & Grima, 2011) provides an opportunity to explore the transports of water masses and anthropogenic carbon, and potential nonlocal large-scale ocean circulation pathways that can sustain regional acidification.

2. Data and Methods

2.1. Analyses of Multidecadal Trends in the Surface Layer of the Warm Pool

For the observational data analyses in this work, we defined the western tropical Pacific Warm Pool as surface water characterized by $T > 28.7$ °C and $S < 34.6$ within the 130–180°E, 5°S–5°N, zonal band. In the central and eastern tropical Pacific, the equatorial divergence brings colder and more saline subsurface waters rich in DIC and nutrients to the surface, with substantial variability in this region also impacting ocean biogeochemistry. The zone of equatorial divergence expands to the western tropical Pacific during the cold phase of the El Niño Southern Oscillation (Figure S1; Ishii et al., 2004, 2014). By contrast, nitrate is depleted and the stratification minimizes the direct impact of the equatorial divergence on the variability of inorganic carbon variables in the Warm Pool. Seasonal as well as interannual variability in inorganic carbon and associated variables is much smaller in the Warm Pool than in the eastern divergence zone (Ishii et al., 2004). It is therefore expected that the trend toward ocean acidification as a result of the increasing anthropogenic CO₂ invasion into the ocean is detectable with observations extending over decades in the Warm Pool.

We used Warm Pool pCO_{2sw} data acquired in a total of 145 cruises conducted since the year 1985 (Table S1). Out of a total of 114 cruises, measurements were made by the Meteorological Research Institute or the Global Environment and Marine Department of Japan Meteorological Agency (JMA) on board JMA's RVs *Ryofu Maru II and III* and *Keifu Maru II* (89 cruises; http://www.data.jma.go.jp/gmd/kaiyou/db/vessel_obs/data-report/html/ship/ship_e.php), on board the *RV Natsushima*, the *RV Kaiyo*, and the *RV Mirai* of the Japan Agency for Marine-Earth Science and Technology (JAMSTEC; 21 cruises; <http://www.godac.jamstec.go.jp/darwin/e>), and on board the University of Tokyo's *RV Hakuho Maru* (4 cruises). In these cruises, an automated underway pCO₂ system equipped with a showerhead-type equilibrator and a nondispersive infrared CO₂ analyzer (Inoue, 2000) was used for the measurements. Mixing ratio of CO₂ in the air of the marine boundary layer has also been measured during these cruises. During 17 cruises conducted between the 1980s and the early 1990s, underway salinity measurements were not carried out and the salinity of surface waters collected at hydrographic stations was therefore used for analysis. Among the other 31 cruises, pCO_{2sw} data were also collected using automated underway systems with different showerhead-type equilibrators (e.g., Feely et al., 1998; Poisson et al., 1993; Wanninkhof & Thoning, 1993; Wong et al., 1993) in 30 cruises, mainly by the U.S. National Oceanic and Atmospheric Administration, and using “rotating disk equilibrator” in one cruise (Sabine et al., 1999). All these data are available in the SOCAT database (Bakker et al., 2016; <https://www.socat.info/index.php/data-access/>).

We analyzed the variability of TA based mainly on TA data calculated from pCO_{2sw} and DIC. Underway measurements of DIC in the western tropical Pacific were performed using a high-precision coulometric technique in conjunction with pCO_{2sw}, temperature, and salinity in 12 cruises of the *RV Kaiyo*, the *RV Mirai*, and the *RV Hakuho Maru* over 1994–2003 (Ishii et al., 2004; <http://www.godac.jamstec.go.jp/darwin/e>). In 31 other cruises conducted in 1994–2016 by the JMA, DIC measurements were made in surface layers at hydrographic stations (http://www.data.jma.go.jp/gmd/kaiyou/db/vessel_obs/data-report/html/ship/ship_e.php). For this total of 43 cruises, TA in surface water was calculated from pCO_{2sw}, DIC, temperature, and salinity data using the concentrations of conservative constituents and equilibrium constants recommended by Dickson et al. (2007) including CO₂ solubility in sea water (Weiss, 1974), dissociation constants for carbonic acid (Lueker et al., 2000), and those for bisulfate ion (Dickson, 1990) and hydrogen fluoride (Dickson & Riley, 1979). The calculations were performed with the Microsoft Excel version of “CO2SYS” (Lewis & Wallace, 1998) modified for use with the carbonic acid dissociation constants given by Lueker et al. (2000). No significant offset was found between the calculated TA and measured TA for data measured by JMA after 2010; the average and standard deviation of the difference in TA (measured-calculated) was $+0.4 \pm 3.7$ μmol · kg⁻¹ ($n = 92$) where ± 3.7 is a standard deviation. The analysis also used quality-controlled TA data from 10 other cruises in the western tropical Pacific conducted by other

organizations since 1992. These data have been incorporated into the GLODAPv2 database (Olsen et al., 2019; https://www.nodc.noaa.gov/ocads/oceans/GLODAPv2_2019/).

TA in the surface layer is known to show little spatial variability over tropical and subtropical zones of the western Pacific when corrected for the dilution and concentration of seawater by precipitation and evaporation by normalizing to a constant salinity value (Millero et al., 1998; Takatani et al., 2014). In this work, salinity-normalized TA at $S = 35$ ($sTA = TA \cdot 35/S$) averaged over the western tropical Pacific during the years 1992–2016 was $2297.2 \pm 3.7 \mu\text{mol} \cdot \text{kg}^{-1}$ ($n = 71$) and showed an indistinct rate of increase ($+0.25 \pm 0.06 \mu\text{mol} \cdot \text{kg}^{-1} \cdot \text{year}^{-1}$, $n = 71$) over the Warm Pool during the years 1992–2016 (Figure 1c). The low variability of sTA in the western tropical Pacific over space and time ($\pm 3.7 \mu\text{mol} \cdot \text{kg}^{-1}$) compares well with the uncertainty of the TA analysis, nominally $6 \mu\text{mol} \cdot \text{kg}^{-1}$ (Tanhua et al., 2010). Therefore, we assume that sTA in surface layer remained unchanged ($2297.2 \pm 3.7 \mu\text{mol} \cdot \text{kg}^{-1}$) over the last three decades since the mid-1980s. Then, values of salinity-normalized DIC ($sDIC = DIC \cdot 35/S$), pH (in total hydrogen ion concentration scale), and saturation indices of calcium carbonate minerals calcite (Ω_{cal}) and aragonite (Ω_{ara}) at in situ temperature and salinity ($\Omega = [\text{Ca}^{2+}][\text{CO}_3^{2-}] K_{\text{sp}}^{-1}$ where K_{sp} is the apparent solubility product of calcite or aragonite (Mucci, 1983)) were calculated from $p\text{CO}_2\text{sw}$, temperature, and salinity data at a constant value of $sTA = 2297.2 \mu\text{mol} \cdot \text{kg}^{-1}$ using the same equilibrium constants and the same algorithms as for the calculation of nTA from $p\text{CO}_2\text{sw}$ and $nDIC$. Finally, their monthly mean values in the Warm Pool were calculated for the months when measurements have been made, and were used to analyze their rates of change and standard errors by a linear least squares method. Each data plot and error bar shown in Figures 1b to 1g denotes monthly mean values and standard deviations.

2.2. Trend Analyses in the Equatorial Undercurrent

For the analyses of multidecadal trends in the Equatorial Undercurrent (EUC), we used hydrographic and biogeochemical data including DIC and TA at depths that have been measured in a narrow equatorial band of the western tropical Pacific (1°S – 1°N , 130°E – 180°). They have been collected over a total of 53 cruises (53 for DIC and 27 for TA) over 1992–2016 including 32 cruises of the JMA and 13 cruises of JAMSTEC (see Table S1). Data from cruises conducted over 1992–2008, that is, 37 cruises for DIC and 13 cruises for TA, were quality-controlled and stored in the PACIFICA databases (Suzuki et al., 2013; <https://www.nodc.noaa.gov/ocads/oceans/PACIFICA/>). Additional measurements during 2009–2016 were taken by JMA over 142°E – 165°E (http://www.data.jma.go.jp/gmd/kaiyou/db/vessel_obs/data-report/html/ship/ship.php). All these data are also available online from GLODAPv2_2019 (Olsen et al., 2019).

A secular trend of increasing DIC following anthropogenic CO_2 invasion into the ocean is detectable as an upward trend of preformed DIC (DIC°), which is the DIC concentration when the water parcel was in last contact with the atmosphere in the surface layer and is represented as

$$\begin{aligned} \text{DIC}^\circ &= \text{DIC}^{\text{opi}} + C_{\text{ant}} \\ &= \text{DIC}^{\text{m}} - \Delta C_{\text{bio}} = \text{DIC}^{\text{m}} - \Delta C_{\text{org}} - \Delta C_{\text{carb}}. \end{aligned} \quad (1)$$

DIC^{opi} refers to preformed DIC in the preindustrial era that is assumed to be in steady state and C_{ant} is the anthropogenic CO_2 component in DIC that increases over time. DIC^{m} is the DIC measured in the ocean interior, and ΔC_{bio} is the correction term for biological activity subsequent to subduction in the formation region. The term ΔC_{bio} is decomposed into the components representing respiration by organisms (remineralization of organic matter), ΔC_{org} , and the dissolution of carbonate particles, ΔC_{carb} , where $\Delta C_{\text{org}} = r_{\text{C}/-\text{O}_2} \cdot \text{AOU}$ and $\Delta C_{\text{carb}} = 0.5 \cdot (\text{TA}^{\text{m}} + r_{\text{N}/-\text{O}_2} \cdot \text{AOU} - \text{TA}^\circ)$; Gruber et al., 1996). Here, AOU refers to the apparent oxygen utilization, that is, the difference between the measured dissolved oxygen concentration and its saturation concentration under the same potential temperature and salinity conditions (García & Gordon, 1992). TA^{m} and TA° are TA measured at depths and preformed TA that has been empirically expressed as a function of potential temperature and other ocean variables (Sabine et al., 2002), respectively. The coefficients $r_{\text{C}/-\text{O}_2}$ and $r_{\text{N}/-\text{O}_2}$ are the stoichiometric C/– O_2 and N/– O_2 remineralization ratios. We used 117/170 for $r_{\text{C}/-\text{O}_2}$ and 16/170 for $r_{\text{N}/-\text{O}_2}$, following the stoichiometric $\Delta P/\Delta N/\Delta C_{\text{org}}/-\Delta \text{O}_2$ ratios of $1/(16 \pm 1)/(117 \pm 14)/(170 \pm 10)$ determined by Anderson and Sarmiento (1994). We also tested $r_{\text{C}/-\text{O}_2}$ of 131/160 and 103/180 and $r_{\text{N}/-\text{O}_2}$ of 17/160 and 15/180 to see the sensitivity of DIC° change to the choice

of $r_{C/-O_2}$ and $r_{N/-O_2}$. Remineralization of organic matter by denitrification is another process contributing to ΔC_{bio} (Sabine et al., 2002). However, we have ignored its contribution in Equation 1, because the contribution of denitrification to DIC changes is considered to be very small over the water column in the western tropical Pacific (Deutsch et al., 2001). Trends of DIC° are also modulated by dilution and concentration of surface water due to precipitation and evaporation. Therefore, we examined the DIC° trend that was normalized to a reference salinity of 35 (sDIC $^\circ$). The rate of sDIC $^\circ$ change was then determined by decomposing it into two terms in Equation 1 as the rate of DIC change corrected for respiration, $DIC^m - \Delta C_{org}$, and that associated with the dissolution of carbonate particles, ΔC_{carb} .

The trend toward increasing sDIC $^\circ$ was analyzed in the thermocline (i.e., in the EUC) and below on potential density horizons spanning $\sigma_\theta = 23.0$ to 27.7 kg m^{-3} (at $\sim 2000 \text{ m}$) in the narrow equatorial band 1°S – 1°N over 130°E – 180° . In the thermocline, both $DIC^m - \Delta C_{org}$ and temperature exhibit large gradients with depth but vertical resolution of discrete water samplings are not sufficient to resolve the vertical profiles well by themselves. Consequently, values of sDIC $^\circ$ on isopycnal horizons have potentially large errors when they are obtained from the interpolated profiles of sDIC $^\circ$ with respect to depth. To reduce their errors associated with the vertical interpolation, we examined the relationship $DIC^m - \Delta C_{org}$, $TA^m + r_{N/-O_2} \cdot AOU$, and TA° , respectively, with respect to potential density (σ_θ ; Figure S2), and they were fitted with a function of σ_θ and observation time by multiple regression analysis:

$$X = c_0 + c_1 \text{ yr} + c_2 \cdot (\sigma_\theta - \sigma_\theta^{\text{ref}}) + c_3 \cdot (\sigma_\theta - \sigma_\theta^{\text{ref}})^2 + \varepsilon, \quad (2)$$

where X denotes $DIC^m - \Delta C_{org}$, $TA^m + r_{N/-O_2} \cdot AOU$, or TA° normalized at $S = 35$, $\text{yr} = \text{year} - 2000$, and ε represents the residual of the fit. The fit was performed on eight density layers, which represent a modest restructuring of the coarse-grained layering presented in a previous study (Sloyan et al., 2003) including Upper Thermocline Water (UTW: 23.0 – $24.5 \text{ kg} \cdot \text{m}^{-3}$), Central Thermocline Water (CTW: 24.5 – $25.5 \text{ kg} \cdot \text{m}^{-3}$), Lower Thermocline Water (LTW: 25.5 – $26.3 \text{ kg} \cdot \text{m}^{-3}$), Thermostat Water (TSW: 26.3 – $26.6 \text{ kg} \cdot \text{m}^{-3}$), Mode Water (MW: 26.6 – $26.9 \text{ kg} \cdot \text{m}^{-3}$), Upper Intermediate Water (UIW: 26.9 – $27.2 \text{ kg} \cdot \text{m}^{-3}$), Lower Intermediate Water (LIW: 27.2 – $27.5 \text{ kg} \cdot \text{m}^{-3}$), and Upper Deep Water (UDW: 27.5 – $27.7 \text{ kg} \cdot \text{m}^{-3}$). Represented as $\sigma_\theta^{\text{ref}}$ in Equation 2 is the reference potential density (midpoint of the density range) for each layer.

Regression analysis was repeated three times for $DIC^m - \Delta C_{org}$ and twice for $TA^m + r_{N/-O_2} \cdot AOU$ and TA° , while rejecting data outside $\pm 2 \text{ s}$. Data of $DIC^m - \Delta C_{org}$, $TA^m + r_{N/-O_2} \cdot AOU$ and TA° were then normalized to the values at $\sigma_\theta^{\text{ref}}$ in each density class using Equation 3:

$$X^{\text{ref}} = X - c_2 \cdot (\sigma_\theta - \sigma_\theta^{\text{ref}}) - c_3 \cdot (\sigma_\theta - \sigma_\theta^{\text{ref}})^2. \quad (3)$$

Finally, cruise-mean values of $(DIC^m - \Delta C_{org})^{\text{ref}}$, $(TA^m + r_{N/-O_2} \cdot AOU)^{\text{ref}}$, and $TA^{\circ\text{ref}}$ were calculated and fitted with a linear function of time for each density class to evaluate the rate of sDIC $^\circ$ change. Equations 2 and 3 were also applied to the data of potential temperature and salinity to evaluate their trends in each density layer in the EUC and below.

2.3. Lagrangian Backward Tracking for the Source Waters of the Warm Pool

Through a series of diagnostics (including Lagrangian) performed on a forward ocean carbon cycle model, we examine anthropogenic CO_2 ventilation and re-emergence pathways and associated transit timescales by highlighting the source waters of the Warm Pool. To do this, we apply the Ariane Lagrangian diagnostic tool kit (Blanke & Grima, 2011) to interpret the model output using circulation fields from a cyclostationary normal-year-forced ORCA2-LIM run that included the PISCES ocean biogeochemistry model run offline (Iudicone et al., 2016). The PISCES component of the model configuration has been run with both the observed anthropogenic CO_2 transient and a preindustrial atmospheric CO_2 boundary, thus facilitating a definition of anthropogenic carbon as the difference between them. For the anthropogenic CO_2 transient thus defined, the model output exhibits a robust correspondence with observational constraints for the year 1995 (Iudicone et al., 2016), namely, a time when a large number of new high-quality ocean carbon data were being acquired globally to assess the total anthropogenic CO_2 inventory in the ocean (Sabine et al., 2004). The advantage of the Lagrangian diagnostics applied to a forward model is that it allows one

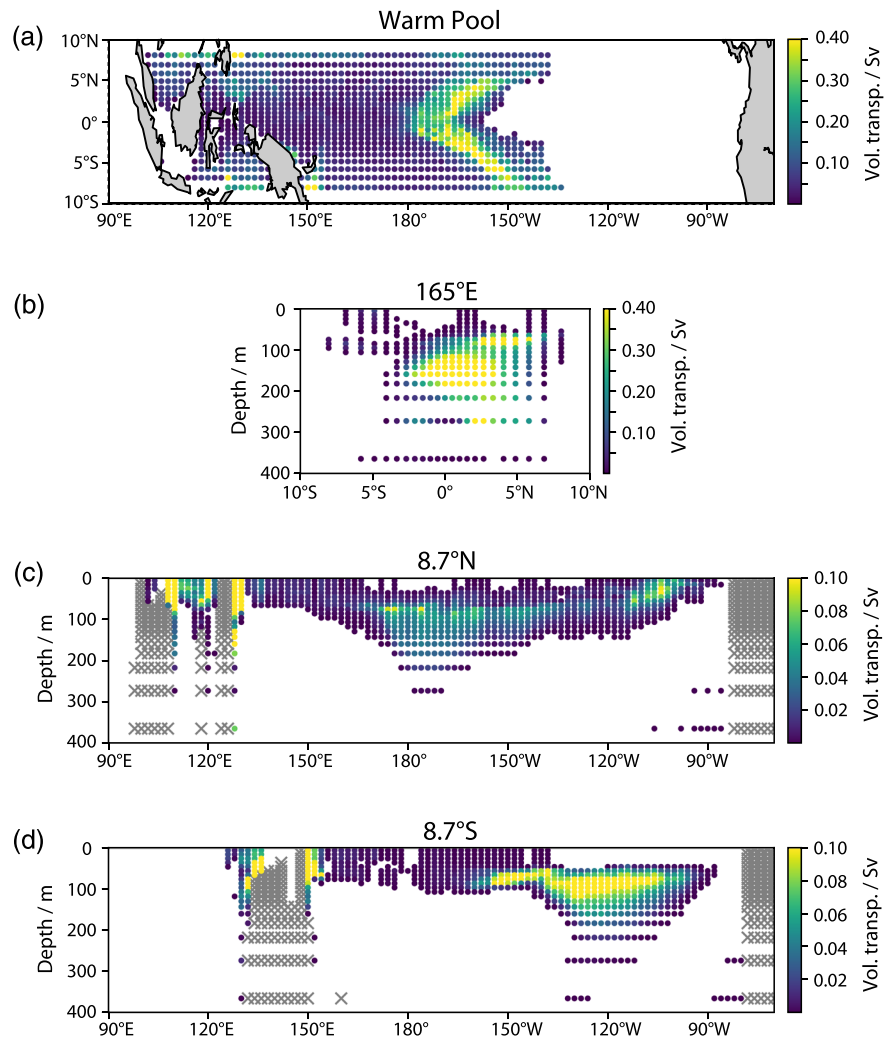


Figure 2. The rate of exchange across the volume bounded below by 28 °C isotherm and to the north and south by the 8.7°N and 8.7°S sections, respectively. (a) Particles seeded on the boundaries and the volume transport in the control volume of the Warm Pool. (b) Distribution of the volume transport across 165°E section that enters the Warm Pool. (c) Distribution of the volume transport across 8.7°N that enters the Warm Pool but not through the EUC at 165°E. (d) Same as (c) but across 8.7°S. This experiment was done with a global ocean circulation model (Judicone et al., 2016) to evaluate the contribution of waters feeding Warm Pool formation in the western tropical Pacific.

to explicitly identify and quantify the flux of the transient anthropogenic component of DIC (C_{ant}), its trajectories (pathways), and advection timescales. The horizontal resolution of the model is nominally 2° in longitude, with the latitudinal resolution varying from 0.5° at the equator to a maximum of 1.9°, with 31 levels vertically. Details of model runs and Lagrangian diagnostics are described elsewhere (Toyama et al., 2017).

3. Results

In the Warm Pool of the western tropical Pacific, surface water is in near-equilibrium with respect to the CO_2 in the atmosphere; that is, $p\text{CO}_{2\text{sw}}$ is generally comparable to $p\text{CO}_{2\text{air}}$ (Figure 1b). This is consistent with what has been reported in previous studies (e.g., Inoue & Sugimura, 1992; Ishii & Inoue, 1995; Takahashi et al., 2009). A moderate range of spatial variability (a few tens of μatm) is seen for $p\text{CO}_{2\text{sw}}$ and can be attributed to the thermodynamic effect of the variability in temperature and salinity as well as local reductions of DIC associated possibly with nitrogen fixation (Ishii et al., 2009; Figure S1). Nevertheless, an upward trend in $p\text{CO}_{2\text{sw}}$ is evident ($+1.37 \pm 0.09 \mu\text{atm year}^{-1}$) over the past three decades of 1985–2016, reflecting the

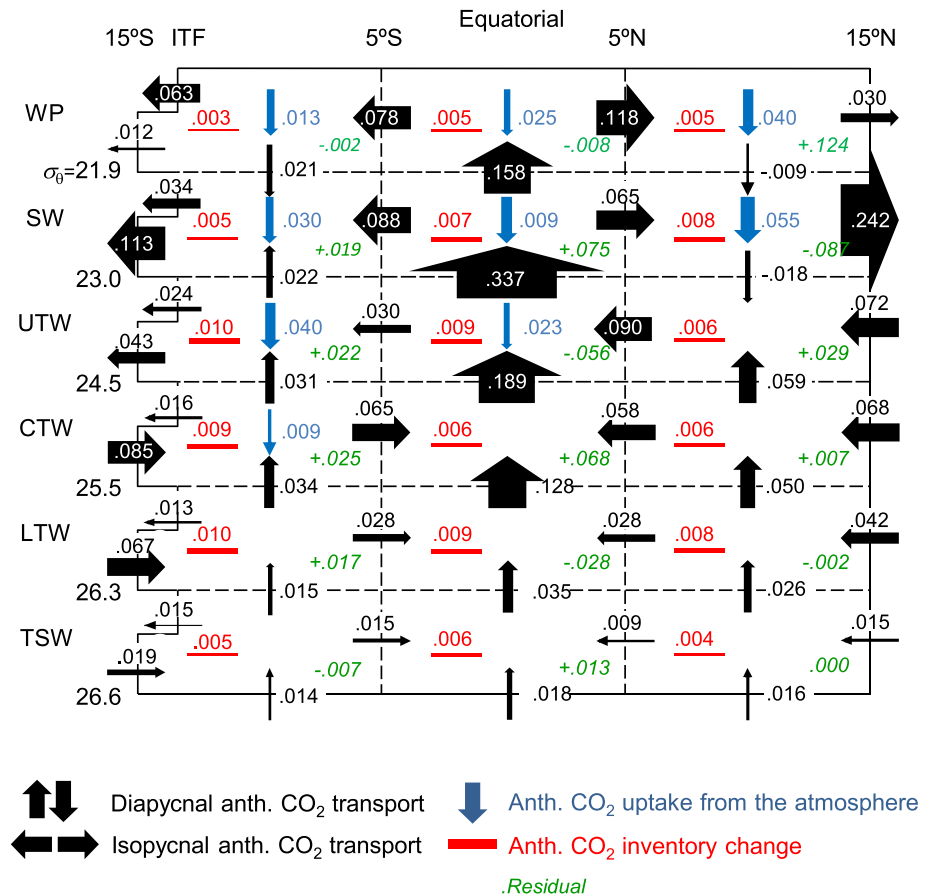


Figure 3. Annual mean exchanges of anthropogenic CO₂ and layer budgets (Pg/year) in the mid-1990s integrated zonally in a density framework over the tropical Pacific (15°S–15°N). The fluxes were identified using biweekly output fields from an ocean carbon cycle model embedded on the ocean circulation model ORCA2-LIM-PISCES (Iudicone et al., 2016). ITF: Indonesian Throughflow; WP: Warm Pool; SW: Surface Water; UTW: Upper Thermocline Water; CTW: Central Thermocline Water; LTW: Lower Thermocline Water; TSW: Thermocline Water. The figure reveals a general pattern of equatorial convergence within the pycnocline (thermocline) layers and a poleward divergence of surface and near-surface waters. Maximum upwelling defined as a cross-isopycnal transport occurs in this coarse-grained layering of the pycnocline across the $\sigma_{\theta} = 23.0$ horizon, with this lying just below the cold tongue in the NINO3 region (90–150°W, 5°S–5°N).

presence of the anthropogenic transient in CO₂ throughout this region. However, its mean rate of increase is significantly lower than that of $p\text{CO}_{2\text{air}}$ for the same period ($+1.74 \pm 0.02 \mu\text{atm year}^{-1}$).

The trend toward increasing $p\text{CO}_{2\text{sw}}$ in the Warm Pool is chemically attributable to the increase of sDIC ($+0.81 \pm 0.06 \mu\text{mol} \cdot \text{kg}^{-1} \cdot \text{year}^{-1}$; Figure 1d). The increase of sDIC also accounts for a lowering of pH ($-0.0013 \pm 0.0001 \text{ year}^{-1}$; Figure 1e) that indicates that the concentration of hydrogen ions has increased on average by 10% in parallel with an 11% increase in $p\text{CO}_{2\text{sw}}$ since 1985. The western tropical Pacific Warm Pool is known to be the region with the highest saturation levels of carbonate minerals (Feely et al., 2009; Jing et al., 2015), providing favorable conditions for calcifying organisms such as corals. However, their saturation levels are also declining with the lowering of pH; Ω_{cal} and Ω_{ara} have decreased at a mean rate of $-0.0125 \pm 0.0010 \text{ year}^{-1}$ and $-0.0083 \pm 0.0007 \text{ year}^{-1}$, respectively, reflecting ocean acidification in this region (Figures 1f and 1g). Nevertheless, their rates of changes are, on the average, ~20% slower than what would be expected if $p\text{CO}_{2\text{sw}}$ were to simply follow the rate of $p\text{CO}_{2\text{air}}$ increase over the same period. The slower rate of acidification identified here in this study contrasts well with the rates determined in the subtropics that are faster and consistent with those expected from the growth rate of $p\text{CO}_{2\text{air}}$ within the uncertainty of analysis (e.g., Bates et al., 2014; González-Dávila et al., 2010;

Midorikawa et al., 2010; Ono et al., 2019). Similar trends of slower oceanic CO₂ increase in the western tropical Pacific have been reported based on the earlier version of SOCAT and an algorithm of TA from salinity and temperature (Lauvset et al., 2015) and based on the time-series measurements of inorganic carbon variables at 137°E section (Ono et al., 2019). The slower oceanic CO₂ increase here has also been projected by Earth System Model simulations used to project the anthropogenically forced trends in the climate system (Resplandy et al., 2013; Schlunegger et al., 2019).

4. Discussion

The observational constraint that the rate of $p\text{CO}_{2\text{sw}}$ increase in the western tropical Pacific Warm Pool is not merely tracking the rate of $p\text{CO}_{2\text{air}}$ increase and is slower than in the subtropics raises the question as to what oceanographic processes modulate the $p\text{CO}_{2\text{sw}}$ increase in this region. In the following subsections, we argue, among the array of processes controlling the rate of sDIC increase, the dominant factor controlling the rate of $p\text{CO}_{2\text{sw}}$, pH, and Ω_{calc} and Ω_{arag} , in the Warm Pool taking the anthropogenic CO₂ transport through the ocean circulation into account and using diagnostics of an ocean modeling and a constraint from inorganic carbon measurements in the ocean interior.

4.1. Transport of Anthropogenic CO₂ in and Around the Tropical Pacific

First, we hypothesize that the renewal time for Warm Pool water is not long enough to reach local air-sea equilibration of CO₂. To test this hypothesis, we considered output from a global ocean circulation model ORCA2-LIM (Iudicone et al., 2016) and defined the 28 °C isotherm as constituting the boundary of Warm Pool waters. Invoking a suite of diagnostics previously applied to identify exchanges across the base of the surface mixed layer (Blanke et al., 2002; Toyama et al., 2017), the exchange rate is estimated across the surface bounded below and to the east by the 28 °C isotherm and to the north and south by sections at 8.7°N and 8.7°S, respectively (Figure 2a). The mean annual net volume transport across the boundaries of this domain is estimated to be 113 Sv ($10^6 \text{ m}^3 \cdot \text{s}^{-1}$), of which a significant fraction is identified at its eastern boundary through the westward South Equatorial Current (SEC; Figure 2a). The volume of the Warm Pool defined here is $1.28 \cdot 10^{15} \text{ m}^3$. The renewal time (volume divided by boundary fluxes) of the Warm Pool volume is thus 131 days, with this being significantly shorter than the air-sea CO₂ equilibration timescale of 1 year in this region (Ishii et al., 2009), indicating that nonlocal ocean dynamical processes can modulate DIC trends and thereby $p\text{CO}_{2\text{sw}}$ in the Warm Pool.

We next analyze the annual budgets in anthropogenic CO₂ for the simulated year 1995 using output from an ocean carbon cycle model (PISCES) run offline using dynamical state variables saved from the ocean circulation model ORCA2-LIM. Here our analysis includes the fluxes across the air-sea interface, increases in layer inventories, and the diapycnal and horizontal transports integrated zonally over the tropical Pacific. The budgets are analyzed in six discrete layers spanning the surface down through the pycnocline (Figure 3). This encompasses the EUC and extends from Warm Pool ($\sigma_{\theta} < 21.9 \text{ kg} \cdot \text{m}^{-3}$) down to the $\sigma_{\theta} = 26.6 \text{ kg} \cdot \text{m}^{-3}$ horizon (depths down to approximately 300 m) in the equatorial band spanning 5°S–5°N, as well in the same density layers in adjacent bands spanning 15–5°S and 5–15°N. These layers have been chosen so as to encompass the critical vertical scales of the shallow subtropical cell overturning. The budget analysis reveals the equatorward convergent transport of anthropogenic CO₂ in the pycnocline from both hemispheres, and subsequent upward diapycnal transport within the equatorial band and divergence in the surface layers including the Warm Pool. The net annual upward diapycnal transport of anthropogenic CO₂ from the upper pycnocline to the surface layer in the 5°S–5°N band amounts to $0.337 \text{ PgC} \cdot \text{year}^{-1}$, and approximately half ($0.158 \text{ PgC} \cdot \text{year}^{-1}$) is transported through the South Equatorial Current (Figure 1a) to the Warm Pool in the surface with associated buoyancy gain by heating and fresh water inputs. The interior exchanges of anthropogenic CO₂ sustained through transports are three to six times larger than the net annual air-to-sea flux of anthropogenic CO₂ from the atmosphere ($0.057 \text{ PgC} \cdot \text{year}^{-1}$) over the same equatorial band. This reveals the predominant role of the upward cross-isopycnal anthropogenic CO₂ transport from the pycnocline for acidification of the surface waters of the equatorial Pacific including the Warm Pool region. Overall, the results are consistent with those considered for the cold tongue region by Zhai et al. (2017).

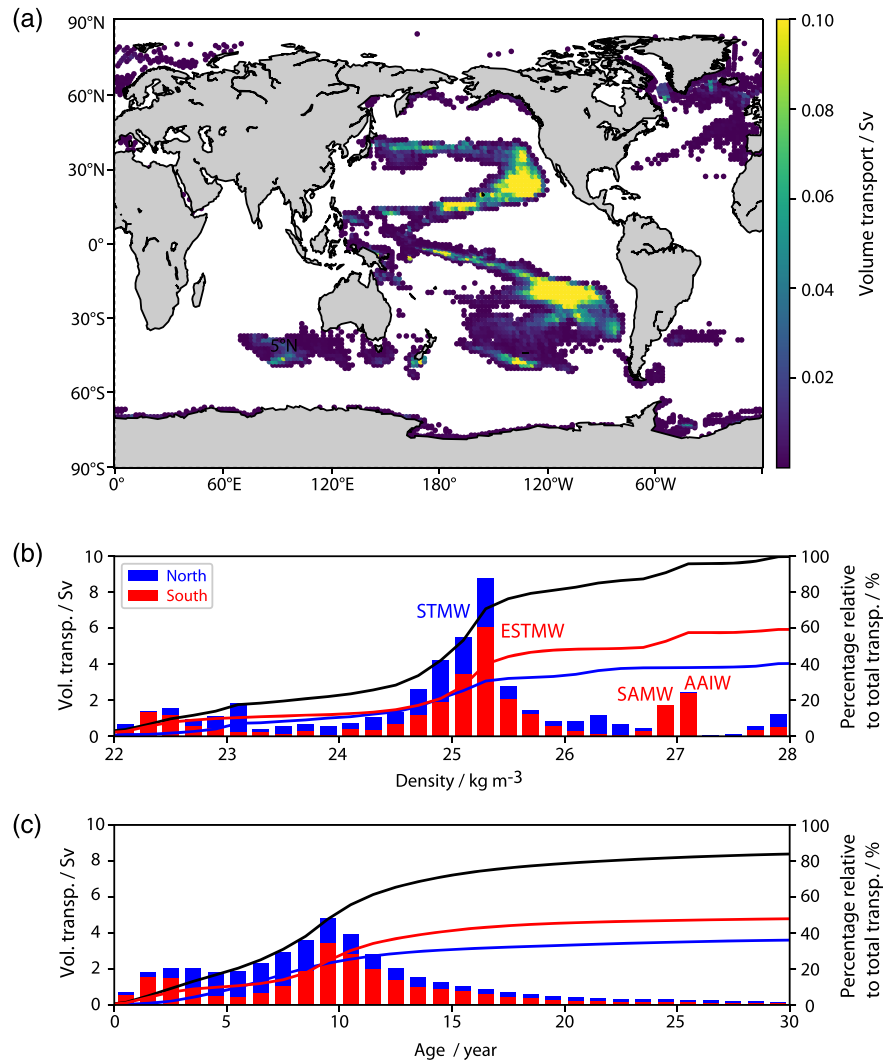


Figure 4. Source waters of the western tropical Pacific Warm Pool that pass through Equatorial Undercurrent across 165°E section identified with Lagrangian diagnostics. (a) Geographical distribution of the origins (downward crossing of surface mixed layer base) of Warm Pool waters with the volume transport shown in the color scale with Eastern Subtropical Mode Water formation regions falling within the local maxima of both hemispheres. (b) Histogram of density of original waters in the Northern Hemisphere (blue) and in the Southern Hemisphere (red) when they crossed the base of the surface mixed layer, and (c) travel times from the EUC at the 165°E section back to the base of mixed layer in the source region. The analysis in (a) and (b) reveal that there are three principal source contributors to the Equatorial Undercurrent: (i) Eastern Subtropical Mode Water from the Southern Hemisphere, (ii) the grouping of Eastern Subtropical Mode Water and Western Subtropical Mode Water in the North Pacific, and the grouping of Subantarctic Mode Water and Antarctic Intermediate Water from the Southern Ocean.

For our third suite of analyses focused on attribution, we have invoked “quantitative mode” functionality in the Ariane Lagrangian diagnostics, where one begins by identifying ocean interior surfaces as starting and stopping regions for large numbers of Lagrangian particles. Importantly, by releasing particles in proportion to the physical transport across an initial section, one can then map the strength of the transports across the final section with a direct mapping to the transports across the original section. In reverse Lagrangian diagnostics (Blanke & Grima, 2011) with the same ocean circulation model (ORCA2-LIM) we identify the pathways by which nonlocal transport of anthropogenic CO₂ impacts the rate of pCO₂sw increase and acidification over the Warm Pool in more detail.

Lagrangian particles were seeded over the 28 °C isotherm bounding the same Warm Pool domain considered for renewal time (Figure 2a). For the case where transport in the forward model was directed into the Warm

Pool, they were then traced backward in time. In the first set of diagnostics, the Lagrangian particles were then stopped when they passed westward across 165°E or reached either the 8.7°N section or the 8.7°S section. This analysis revealed that 50 Sv (44%) of the net transport into the Warm Pool crossed 165°E section within the EUC below the Warm Pool (Figure 2b), with subsequent near-surface and surface entrainment into the westward-flowing SEC and concurrent gain of buoyancy. For this pathway, nearly 73% of the waters take less than 3 years between crossing 165°E section within the EUC and entering the Warm Pool. The remaining 63 Sv (56%) of the transport of the flux into the Warm Pool arrives directly through equatorward pycnocline convergence with subsequent near-surface and surface entrainment into the SEC or through the low latitude western boundary currents of both hemispheres such as Mindanao Current and New Guinea Coastal Current (Fine et al., 1994) without passing through the EUC at 165°E (Figures 2c and 2d). Among the 63 Sv, 36 Sv is transported from the northern hemisphere across the 8.7°N section (Figure 2c) and the other 27 Sv is transported from the southern hemisphere across the 8.7°S section (Figure 2d).

In the second run of the Lagrangian diagnostics, the Lagrangian particles that crossed the 165°E section within the EUC were then re-released at their stopping points from the first step of the Lagrangian calculations along 165°E in order to identify their subduction source regions, that is, their first points of intersection with the mixed layer in both hemispheres (Figure 4a). There, we identify the EUC waters as having three main sources: (i) Eastern Subtropical Mode Water (Hanawa & Talley, 2001) in the South Pacific with formation density of 24.8–25.6 kg · m⁻³ formed on the eastern periphery of the subtropical gyre, (ii) Western and Eastern Subtropical Mode Waters in the North Pacific with formation density of 24.8–25.4 kg · m⁻³ formed on the northern and eastern periphery of the subtropical gyre, and (iii) Subantarctic Mode Water and Antarctic Intermediate Water with formation densities of 26.8–27.2 kg · m⁻³. The range of transit times for particles from these subduction regions to reach the EUC at 165°E is broad, with 83% taking more than 5 years and a median of 8.7 years. Nevertheless, they transported a total of 0.74 PgC · year⁻¹ of anthropogenic CO₂ to the Warm Pool in 1995.

The origins of the Warm Pool water that does not pass through the EUC at 165°E is also broadly distributed (Figure S3a) and these waters transport a total of 1.02 PgC · year⁻¹ of anthropogenic CO₂. However, the transit time to reach the 8.7°S or 8.7°N sections tends to be shorter, with 68% of these waters taking less than 5 years. Overall, 47% of the source waters take more than 5 years to reach the EUC at 165°E or the sections at 8.7°N/S. The pathway of anthropogenic CO₂ transport to the Warm Pool entails intergyre exchange of thermocline waters associated with subtropical overturning structures (Nakano et al., 2015; Rodgers et al., 2003), which generally take a decade or more. This is consistent with ventilation ages of 5 to 20 years in the tropical Pacific thermocline inferred from the measurements of dissolved chlorofluorocarbons (Fine et al., 2001).

4.2. Trend of DIC Increase in the EUC

As our analysis reveals that the EUC is a principal conduit sustaining acidification of the Warm Pool, we are motivated to consider observational constraints on the EUC waters themselves dating back to the early 1990s. The analysis thus encompasses an era when high-quality data of DIC and TA are available due to improved measurement technique using coulometry for DIC (Johnson et al., 1985) and data quality control using Certified Reference Material for DIC and TA measurements (Dickson, 2010) as well as a secondary data quality control by the method of crossover analyses of vertical profiles from different cruises (Olsen et al., 2019; Tanhua et al., 2010) facilitating reliable identification of decadal trends.

It is found that the increase of DIC^m – ΔC_{org} in Equation 1 is evident and accounts predominantly for the increase in sDIC^o in the upper layers of the western tropical Pacific (Figure 5 and Table 1). In contrast, the changes in ΔC_{carb} are minimal and insignificant. In the pycnocline, the linear rate of sDIC^{oref} change for the years 1992–2016 ranged between +0.52 ± 0.09 μmol · kg⁻¹ · year⁻¹ in LTW and +0.72 ± 0.10 μmol · kg⁻¹ · year⁻¹ in CTW (Table 1). These estimates of sDIC^o change are not sensitive to the stoichiometric ΔN/ΔC_{org}/–ΔO₂ ratio we use (Table S2). Below the pycnocline where AOU is larger and more variable than in the pycnocline, the estimates of sDIC^o change are more sensitive to the choice of ΔN/ΔC_{org}/–ΔO₂ ratio. However, it is evident that the mean rate of sDIC^o change is lower in deeper layers. These results indicate the increasing transport of anthropogenic CO₂ being accumulated nonlocally through the EUC. The rates of sDIC^o increase in the EUC are comparable or slightly lower than the mean rate of

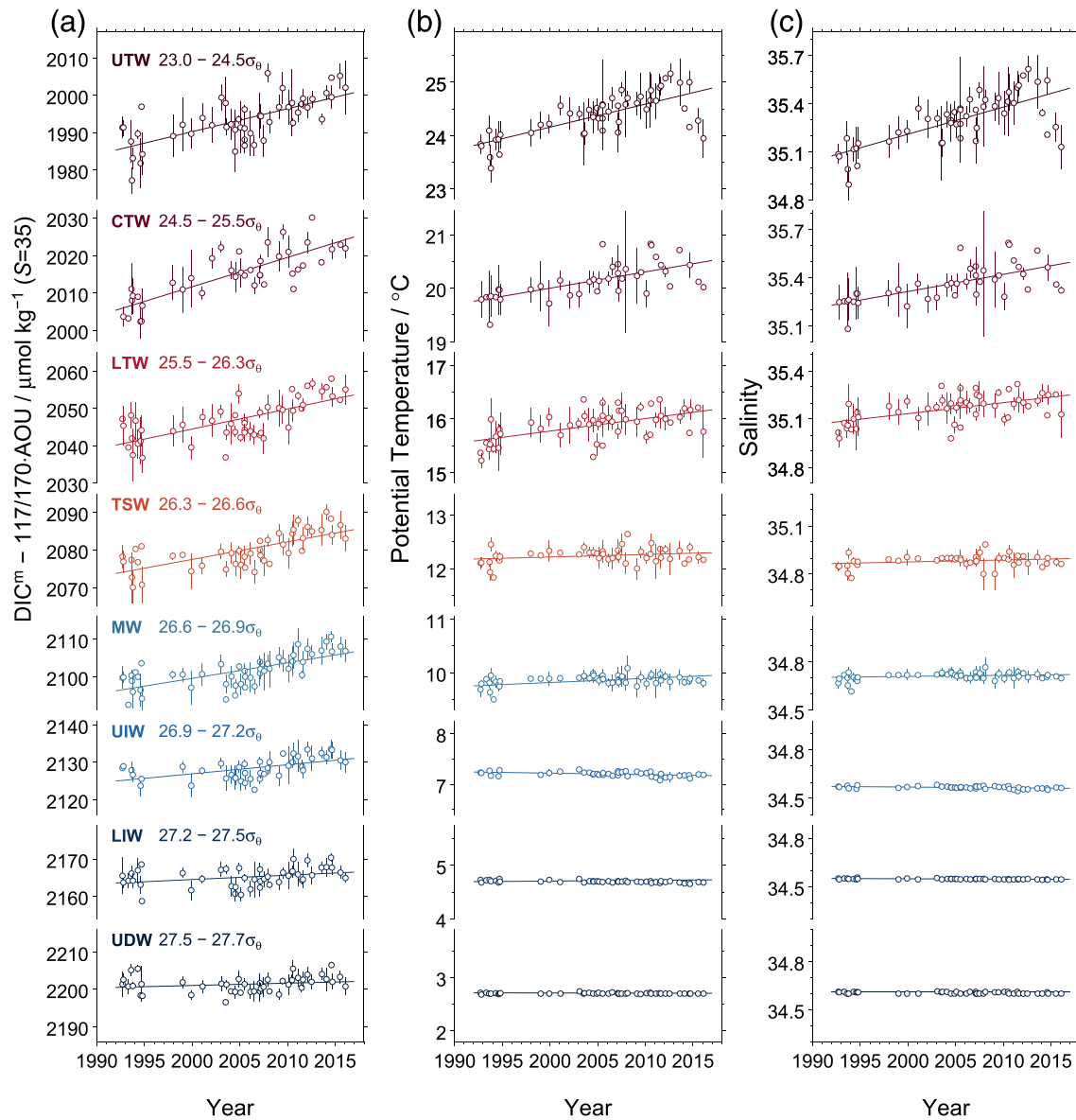


Figure 5. Trends on isopycnal layers in the Equatorial Undercurrent (EUC) for the years 1992–2016. (a) Salinity-normalized respiration-corrected DIC ($\text{DIC}^m - \Delta C_{\text{org}}$), (b) potential temperature, and (c) salinity. These trends were analyzed for the western Pacific equatorial band (130°E – 180° , 1°S – 1°N) on eight discrete layers in the EUC and below (see sections 2.2 and 2.3). Each data plot and its error bar denote cruise-mean value and its standard deviation, respectively.

sDIC increase in the overlying waters of the Warm Pool over the same period, namely, since the early 1990s ($+0.77 \pm 0.08 \mu\text{mol} \cdot \text{kg}^{-1} \cdot \text{year}^{-1}$). This is consistent with our inference from the model diagnostics described in the previous section that the acidification of the Warm Pool is primarily supported by intergyre transport of anthropogenic CO_2 within the thermocline through the EUC, with the predominant anthropogenic CO_2 content of these waters crossing the air-sea interface in the subtropics.

4.3. Attribution of Slower Ocean Acidification in the Warm Pool

To better constrain how ocean acidification in the western tropical Pacific may evolve in the future, it is important to identify mechanistically why the mean rate of $p\text{CO}_2\text{sw}$ increase in this region has been slower than that of $p\text{CO}_2\text{air}$. As was emphasized in the previous section, one candidate process involves the time lag associated with intergyre exchange of thermocline waters. The CO_2 increase in the atmosphere accelerated

Table 1

Mean Rates of Change \pm Standard Error ($\mu\text{mol} \cdot \text{kg}^{-1} \cdot \text{year}^{-1}$) in the Components of Salinity-Normalized Preformed DIC (sDIC^o) in the Interior of the Western Pacific Equatorial Band (130°E–180°, 1°S–1°N) for the Years 1992–2016

Name	Density range	(DIC ^m – ΔC _{org}) ^{ref}	<i>n</i>	ΔC _{carb} ^{ref†}	<i>n</i>	sDIC ^{o ref}
UTW	23.0–24.5σ _θ	+0.62 ± 0.09*	50	+0.04 ± 0.04	23	+0.58 ± 0.10
CTW	24.5–25.5σ _θ	+0.74 ± 0.09*	40	+0.03 ± 0.05	20	+0.72 ± 0.10
LTW	25.5–26.3σ _θ	+0.53 ± 0.08*	51	+0.01 ± 0.04	23	+0.52 ± 0.09
TSW	26.3–26.6σ _θ	+0.47 ± 0.07*	44	+0.00 ± 0.05	23	+0.47 ± 0.09
MW	26.6–26.9σ _θ	+0.42 ± 0.06*	50	–0.03 ± 0.05	23	+0.44 ± 0.08
UIW	26.9–27.2σ _θ	+0.24 ± 0.06*	43	–0.13 ± 0.07	20	+0.37 ± 0.09
LIW	27.2–27.5σ _θ	+0.11 ± 0.05*	44	–0.05 ± 0.04	25	+0.16 ± 0.06
UDW	27.5–27.7σ _θ	+0.07 ± 0.05	44	–0.08 ± 0.05	23	+0.14 ± 0.06

Note. Stoichiometric ratios of ΔN/ΔC_{org}/–ΔO₂ = 16/117/170 (Anderson & Sarmiento, 1994) were used for the calculation of sDIC^o.

Abbreviations: CTW, Central Thermocline Water; LIW, Lower Intermediate Water; LTW, Lower Thermocline Water; MW, Mode Water; TSW, Thermocline Water; UDW, Upper Deep Water; UIW, Upper Intermediate Water; UTW, Upper Thermocline Water.

*Statistically significant (*p* < 0.05). †ΔC_{carb}^{ref} = 0.5 · {(TA^m + *r*_{N/–O₂} · AOU)^{ref} – TA^{o ref}}.

at a mean rate of $+0.26 \pm 0.05 \text{ ppm} \cdot \text{decade}^{-2}$ over 1959–2010 (Ballantyne et al., 2012) or $+0.29 \pm 0.07 \text{ ppm} \cdot \text{decade}^{-2}$ over 1985–2015 (WMO, 2017) on average due to increasing anthropogenic CO₂ emissions. An interior residence time of order one decade during the transport from the extratropics to the EUC means that atmospheric CO₂ increased subsequent to the water parcel losing contact with the atmosphere in the extratropics before reentering through reemergence into the surface layer of the tropics. Consequently, the less rapid rate of *p*CO_{2sw} increase than that of *p*CO_{2air} in the Warm Pool would reflect the memory of water parcels from a time when the atmospheric *p*CO_{2air} increase was slower. This in turn suggests that if policy changes were to lead to carbon removal from the ocean, reversing the sign of Δ*p*CO₂ over large scales, there would nevertheless be a delay in the response of the Warm Pool acidification state determined by the intergyre exchange timescale for equatorial thermocline waters.

Another candidate mechanism for the slower *p*CO_{2sw} increases in the Warm Pool than that expected from the growth rate of *p*CO_{2air} for the same period could be associated with the change in the ocean circulation, that is, an increase in the relative contribution of waters from Southern Hemisphere to the Warm Pool through the EUC. For a given thermocline density in the mean state, the southern source waters of the EUC are not only warmer and saltier but also characterized by lower DIC^o (Figure S4). Notably, salinity has been increasing over recent decades within the EUC (Figure 5c). This provides potential observational support for an increase in the relative contribution of the southern source to the EUC, and therefore a slowing of the rate of sDIC^o increase. The mean rate of salinity increase over time is the highest in the UTW ($+0.171 \pm 0.024 \text{ decade}^{-1}$ in σ_θ = 23.0 to 24.5 kg · m^{–3}; Table S3). This could be accompanied by a change of $-0.31 \pm 0.14 \mu\text{mol} \cdot \text{kg}^{-1} \cdot \text{year}^{-1}$ of DIC^o, which offsets the DIC^o increase due to anthropogenic CO₂ accumulation, for the case where the increase in salinity reflects the increase in volume transport from the south. Nevertheless, there are caveats to this interpretation. First, increases in salinity observed in the EUC could be sustained by increases in the salinity of waters emanating from either hemisphere (Hosoda et al., 2009). Second, the slower sDIC^o increase in the EUC than that expected from the *p*CO_{2air} growth rate may in part also reflect the shoaling and warming of density layers associated with the salinity increase. Third, in the UTW where the mean rate of salinity increase was the highest, salinity dropped in 2015 to the level in the 1990s but sDIC^o continued to increase, suggesting that the changes in salinity were not tightly coupled with the changes in the relative contribution of waters from Southern Hemisphere to the EUC and thereby the changes in sDIC^o. Better mechanistic understanding of why salinity is changing in the EUC is needed to understand how salinity changes and sDIC^o increases are linked there.

5. Conclusions

Invoking data synthesis products built upon oceanic CO₂ measurements, we have identified a trend toward increasing surface ocean CO₂ and an associated acidification in the tropical Pacific Warm Pool, revealing $+1.37 \pm 0.09 \mu\text{atm} \cdot \text{year}^{-1}$ for *p*CO_{2sw}, $+0.81 \pm 0.06 \mu\text{mol} \cdot \text{kg}^{-1} \cdot \text{year}^{-1}$ for sDIC, $-0.0013 \pm 0.0001 \text{ year}^{-1}$ for pH, and $-0.0083 \pm 0.0007 \text{ year}^{-1}$ for Ω_{ara} for the years 1985–2016. For this critically important

Acknowledgments

This work was not possible without the efforts of many officers, crew, scientists, and technicians aboard the cruises for research and the Ship of Opportunity who acquired the high-quality oceanographic data. We are also grateful to Burke Hales and an anonymous reviewer for their insightful suggestions. The data of ocean carbon measurements we used in this work are freely accessible through the websites of JMA (http://www.data.jma.go.jp/gmd/kaiyou/db/vessel_obs/data-report/html/ship/ship_e.php), JAMSTEC (<http://www.godac.jamstec.go.jp/darwin/e>), SOCAT (<https://www.socat.info/index.php/data-access/>), PACIFICA (<https://www.nodc.noaa.gov/ocads/oceans/PACIFICA/>), and GLODAP (https://www.nodc.noaa.gov/ocads/oceans/GLODAPv2_2019/). The ocean circulation model ORCA2-LIM and the ocean carbon cycle model PISCES are the components of a framework of ocean-related engines “The Nucleus for European Modelling of the Ocean (NEMO)” (<https://www.nemo-ocean.eu/framework/components/engines/>). The Ariane Lagrangian diagnostic tool is available at <http://stockage.univ-brest.fr/~grima/Ariane/>. Processed data sets and modeling outputs including time series data of inorganic carbon variables in surface seawater and partial pressure of CO₂ in the atmosphere in the Warm Pool region presented in Figure 1, data of vertical profiles of respiration-corrected sDIC and sTA in the western Pacific equatorial zone shown in Figure S2, time series data of respiration-corrected sDIC on reference potential density in the EUC shown in Figure 5 and those of respiration-corrected sTA and preformed sTA, and outputs of PISCES run using circulation fields from a cyclostationary normal-year-forced ORCA2-LIM run, and the results of its diagnostics as shown in Figures 2, 4, and S3, are available through http://dogfish.princeton.edu/ACIDIFICATION_BELOW/. M.I., K.T., D.S., N.K., H.O., K.E., and T.N. thank support from Meteorological Research Institute’s research fund C4 for the study of ocean biogeochemistry and acidification and MEXT KAKENHI grant JP15H05818, 16H01594, and 19H05700. Support for K.B.R. came through the Institute for Basic Science project code IBS-R028-D1. This is contribution 4901 from the Pacific Marine Environmental Laboratory of NOAA. Ocean CO₂ data synthesis team of PACIFICA supported by PICES and those of SOCAT and GLODAPv2 supported by many programs and organizations under the auspices of

biodiversity hot spot region, this translates to an acidification rate that is on average ~20% lower than what would be expected if the surface ocean were to simply follow the growth rate of CO₂ in the overlying atmosphere ($+1.74 \pm 0.02 \mu\text{atm} \cdot \text{year}^{-1}$). Through the combined use of observations and modeling tools (with a joint Eulerian/Lagrangian analysis), our results implicate the importance of anthropogenic CO₂ transport through the Subtropical Cells and the EUC in sustaining and regulating the rate of acidification in Warm Pool surface waters.

Taken together our model attribution exercise reveals that “ocean acidification from below” is a framework that applies not only to the Warm Pool but also more generally over the equatorial band via the equatorial divergence zone to the east. Specifically, it implies a key role of ocean circulation as well as the growth rate of the mixing ratio of CO₂ in the atmosphere in modulating the rate of ocean acidification. Our mechanistic attribution also provides insight into the more general circulation structures and pathways sustaining acidification in future climate projections with Earth System Models (Resplandy et al., 2013). Nevertheless, the importance of ocean acidification from below should not be assumed to be limited to the equatorial Pacific. Its importance has been suggested for the acidification on the continental shelf along the west coast of North America (Feely et al., 2008; Harris et al., 2013; Hauri et al., 2013). Furthermore, using the same cyclostationary ocean carbon cycle model configuration applied here, the study of Toyama et al. (2017) highlighted a number of regions over the global ocean domain, including western boundary current regions where re-emergence rates of anthropogenic CO₂ into the surface mixed layer from the thermocline are larger than local air-sea CO₂ fluxes. Among the regions highlighted by Toyama et al. (2017), the western tropical Pacific Warm Pool is special in that it exhibits a higher signal-to-noise ratio for the trend in acidification rate due to the relatively weak seasonal and interannual variability there in the inorganic carbon variables. The weak seasonal and interannual variability there is interpreted to be due to the effect of cumulative DIC removal through biological production driving nitrate-depletion. Biological removal of DIC due to nitrate-depletion operates as a low-pass filter for DIC with this magnitude being modulated in response to the change in the strength of upwelling of pycnocline waters and renders the trend of acidification being affected by the “aged” waters from below emergent in the Warm Pool much earlier than in the cold tongue region. Although a number of technical and resource challenges exist for applying the methods developed here to evaluate full transient cases with high resolution models, the insights afforded with the analysis methods presented here demonstrate their value for broader applications pertaining to resource management and climate questions.

References

- Albright, R., Takeshita, Y., Koweek, D. A., Ninokawa, A., Wolfe, K., Rivlin, T., et al. (2018). Carbon dioxide addition to coral reef waters suppresses net community calcification. *Nature*, 555, 516–519. <https://doi.org/10.1038/nature25968>
- Anderson, L. A., & Sarmiento, J. L. (1994). Redfield ratios of remineralization determined by nutrient data analysis. *Global Biogeochemical Cycles*, 8, 65–80. <https://doi.org/10.1029/93GB03318>
- Bakke, D. C. E., Pfeil, B., Landa, C. S., Metzl, N., O’Brien, K. M., Olsen, A., et al. (2016). A multi-decade record of high quality fCO₂ data in version 3 of the Surface Ocean CO₂ atlas (SOCAT). *Earth System Science Data*, 8, 383–413. <https://doi.org/10.5194/essd-8-383-2016>
- Ballantyne, A. P., Alden, C. B., Miller, J. B., Tans, P. P., & White, J. W. C. (2012). Increase in observed net carbon dioxide uptake by land and oceans during the past 50 years. *Nature*, 488, 70–72. <https://doi.org/10.1038/nature11299>
- Bates, N. R., Astor, Y. M., Church, M. J., Currie, K., Dore, J. E., Gonzalez-Davila, M., et al. (2014). A time-series view of changing ocean chemistry due to ocean uptake of anthropogenic CO₂ and ocean acidification. *Oceanography*, 27, 126–141. <https://doi.org/10.5670/oceanog.2014.16>
- Blanke, B., & Grima, N. (2011). *ARIANE v2.2.6*. CNRS/IUEM/Université de Bretagne Occidentale/IRD/Ifremer/Laboratoire de Physique des Océans. Retrieved from <http://stockage.univ-brest.fr/~grima/Ariane/>
- Blanke, B., Speich, S., Madec, G., & Mauge, R. (2002). A global diagnostic of interior ocean ventilation. *Geophysical Research Letters*, 29(8), 133884817. <https://doi.org/10.1029/2001GL013727>
- Burke, L., Reyter, K., Spalding, M., & Perry, A. (2011). *Reefs at risk revisited*. Washington D. C: World Resources Institute. <https://www.wri.org/publication/reefs-risk-revisited>
- Burke, L., Reyter, K., Spalding, M., & Perry, A. (2012). *Reefs at risk revisited in the coral triangle*. Washington, DC: World Resources Institute. <http://www.wri.org/publication/reefs-risk-revisited-coral-triangle>
- Deutsch, C., Gruber, N., Key, R. M., Sarmiento, J. L., & Ganachaud, A. (2001). Denitrification and N₂ fixation in the Pacific Ocean. *Global Biogeochemical Cycles*, 15, 483–506. <https://doi.org/10.1029/2000GB001291>
- Dickson, A. G. (1990). Standard potential of the reaction: AgCl(s) + ½H₂(g) = Ag(s) + HCl(aq), and the standard acidity constant of the ion HSO₄⁻ in synthetic sea water from 273.15 to 318.15 K. *Journal of Chemical Thermodynamics*, 22, 113–127. [https://doi.org/10.1016/0021-9614\(90\)90074-Z](https://doi.org/10.1016/0021-9614(90)90074-Z)
- Dickson, A. G. (2010). Standards for ocean measurements. *Oceanography*, 23, 34–47. <https://doi.org/10.5670/oceanog.2010.22>
- Dickson, A. G., & Riley, J. P. (1979). The estimation of acid dissociation constants in seawater media from potentiometric titrations with strong base. I. the ionic product of water (K_w). *Marine Chemistry*, 7, 89–99. [https://doi.org/10.1016/0304-4203\(79\)90001-X](https://doi.org/10.1016/0304-4203(79)90001-X)

IOCCP, SOLAS, and IMBeR are also acknowledged.

- Dickson, A. G., Sabine, C. L., & Christian, J. R. (Eds) (2007). Guide to best practices for ocean CO₂ measurements. *PICES Special Publication*, 3, 191. <https://doi.org/10.1039/9781847550835>
- Feely, R. A., Doney, S. C., & Cooley, S. R. (2009). Ocean acidification: Present conditions and future changes in a high-CO₂ world. *Oceanography*, 22, 36–47. <https://doi.org/10.5670/oceanog.2009.95>
- Feely, R. A., Sabine, C. L., Hernandez-Ayon, J. M., Ianson, D., & Hales, B. (2008). Evidence for upwelling of corrosive “acidified” water onto the continental shelf. *Science*, 320(5882), 1490–1492. <https://doi.org/10.1126/science.1155676>
- Feely, R. A., Takahashi, T., Wanninkhof, T. R., McPhaden, M. J., Cosca, C. E., Sutherland, S. C., & Carr, M. E. (2006). Decadal variability of the air-sea CO₂ fluxes in the equatorial Pacific Ocean. *Journal of Geophysical Research*, 111, C08S90. <https://doi.org/10.1029/2005JC003129>
- Feely, R. A., Wanninkhof, R., Milburn, H. B., Cosca, C. E., Stapp, M., & Murphy, P. P. (1998). A new automated underway system for making high precision pCO₂ measurements onboard research ships. *Analytica Chimica Acta*, 377, 185–191. [https://doi.org/10.1016/S0003-2670\(98\)00388-2](https://doi.org/10.1016/S0003-2670(98)00388-2)
- Feely, R. A., Wanninkhof, R., Takahashi, T., & Tans, P. (1999). Influence of El Niño on the equatorial Pacific contribution to atmospheric CO₂ accumulation. *Nature*, 398, 597–601. <https://doi.org/10.1038/19273>
- Fine, R. A., Lukas, R., Bingham, F. M., Warner, M. J., & Gammon, R. H. (1994). The western equatorial Pacific: A water mass crossroads. *Journal of Geophysical Research*, 99, 25,063–25,080. <https://doi.org/10.1029/94JC02277>
- Fine, R. A., Mailliet, K. A., Sullivan, K. F., & Willey, D. (2001). Circulation and ventilation flux of the Pacific Ocean. *Journal of Geophysical Research*, 106, 22,159–22,178. <https://doi.org/10.1029/1999JC000184>
- García, H. E., & Gordon, L. I. (1992). Oxygen solubility in seawater: Better fitting equations. *Limnology and Oceanography*, 37, 1307–1312. <https://doi.org/10.4319/lo.1992.37.6.1307>
- Gattuso, J.-P., Magnan, A., Billé, R., Cheung, W. W. L., Howes, E. L., Joos, F., et al. (2015). Contrasting futures for ocean and society from different anthropogenic CO₂ emissions scenarios. *Science*, 349(6243), aac4722. <https://doi.org/10.1126/science.aac4722>
- González-Dávila, M., Santana-Casiano, J. M., Rueda, M. J., & Llinás, O. (2010). The water column distribution of carbonate system variables at the ESTOC site from 1995 to 2004. *Biogeosciences*, 7, 3067–3081. <https://doi.org/10.5194/bg-7-3067-2010>
- Gruber, N., Sarmiento, J. L., & Stocker, T. F. (1996). An improved method for detecting anthropogenic CO₂ in the oceans. *Global Biogeochemical Cycles*, 10, 809–837. <https://doi.org/10.1029/96GB01608>
- Hanawa, K., & Talley, L. (2001). Mode waters. In G. Siedler, J. Church, & J. J. Gould (Eds.), *Ocean circulation and climate, International Geophysics Series* (Vol. 77, pp. 373–386). San Diego, CA: Academic.
- Harris, K. E., DeGrandpre, M. D., & Hales, B. (2013). Aragonite saturation states in a coastal upwelling zone. *Geophysical Research Letters*, 40, 2720–2725. <https://doi.org/10.1002/grl.50460>
- Hauri, C., Gruber, N., Vogt, M., Doney, S. C., Feely, R. A., Lachkar, Z., et al. (2013). Spatiotemporal variability and long-term trends of ocean acidification in the California Current System. *Biogeosciences*, 10, 193–216. <https://doi.org/10.5194/bg-10-193-2013>
- Hoegh-Guldberg, O., Mumby, P. J., Hooten, A. J., Steneck, R. S., Greenfield, P., Gomez, E., et al. (2007). Coral reef under rapid climate change and ocean acidification. *Science*, 318, 1737–1742. <https://doi.org/10.1126/science.1152509>
- Hosoda, S., Suga, T., Shikama, N., & Mizuno, K. (2009). Global surface salinity change detected by Argo and its implication for hydrological cycle intensification. *Journal of Oceanography*, 65, 579–586. <https://doi.org/10.1007/s10872-009-0049-1>
- Inoue, H. Y. (2000). CO₂ exchange between the atmosphere and the ocean: Carbon cycle studies of the Meteorological Research Institute since 1968. In N. Handa, E. Tanoue, & T. Hama (Eds.), *Dynamics and characterization of marine organic matter: Ocean sciences research book series* (Vol. 2, pp. 509–531). Tokyo: Terra scientific/springer. <https://doi.org/10.1007/978-94-017-1319-1>
- Inoue, H. Y., Matsueda, H., Ishii, M., Fushimi, K., Hirota, M., Asanuma, I., & Takasugi, Y. (1995). Long-term trend of the partial pressure of carbon dioxide (pCO₂) in surface waters of the western North Pacific, 1984–1993. *Tellus, Series B*, 47, 391–413. <https://doi.org/10.3402/tellusb.v47i4.16057>
- Inoue, H. Y., & Sugimura, Y. (1992). Variations and distributions of CO₂ in and over the equatorial Pacific during the period from the 1986/88 El Niño event to the 1988/89 La Niña event. *Tellus, Series B*, 44, 1–22. <https://doi.org/10.3402/tellusb.v44i1.15417>
- Ishii, M., Feely, R. A., Rodgers, K. B., Park, G.-H., Wanninkhof, R., Sasano, D., et al. (2014). Air-sea CO₂ flux in the Pacific Ocean for the period 1990–2009. *Biogeosciences*, 11(3), 709–734. <https://doi.org/10.5194/bg-11-709-2014>
- Ishii, M., & Inoue, H. Y. (1995). Air-sea exchange of CO₂ in the central and western equatorial Pacific in 1990. *Tellus, Series B*, 47, 447–460. <https://doi.org/10.1034/j.1600-0889.47.issue4.5.x>
- Ishii, M., Inoue, H. Y., Midorikawa, T., Saito, S., Tokieda, T., Sasano, D., et al. (2009). Spatial variability and decadal trend of the oceanic CO₂ in the western equatorial Pacific warm/fresh water. *Deep-Sea Research, Part II*, 56(8–10), 591–606. <https://doi.org/10.1016/j.dsr2.2009.01.002>
- Ishii, M., Saito, S., Tokieda, T., Kawano, T., Matsumoto, K., & Inoue, H. Y. (2004). Variability of surface layer CO₂ parameters in the western and central equatorial Pacific. In M. Shiyomi, H. Kawahata, H. Koizumi, A. Tsuda, & Y. Awaya (Eds.), *Global Environmental Change in the Ocean and on Land* (pp. 59–94). Tokyo: Terrapub.
- Iudicone, D., Rodgers, K. B., Plancherel, Y., Aumont, O., Ito, T., Key, R. M., et al. (2016). The formation of the ocean’s anthropogenic carbon reservoir. *Scientific Reports*, 6, 35473. <https://doi.org/10.1038/srep35473>
- Jing, L.-Q., Feely, R. A., Carter, B. R., Greeley, D. J., Gledhill, D. K., & Arzayus, K. M. (2015). Climatological distribution of aragonite saturation state in the global oceans. *Global Biogeochemical Cycles*, 29, 1656–1673. <https://doi.org/10.1002/2015GB005198>
- Johnson, K. M., King, A. E., & Sieburth, J. M. (1985). Coulometric TCO₂ analyses for marine studies; an introduction. *Marine Chemistry*, 16, 61–82. [https://doi.org/10.1016/0304-4203\(85\)90028-3](https://doi.org/10.1016/0304-4203(85)90028-3)
- Key, R. M., Sabine, C. L., Lee, K., Wanninkhof, R., Bullister, J., Feely, R. A., et al. (2004). A global ocean carbon climatology: Results from Global Data Analysis Project (GLODAP). *Global Biogeochemical Cycles*, 18, GB4031. <https://doi.org/10.1029/2004GB002247>
- Kleypas, J. A., Buddemeier, R. W., Archer, D., Gattuso, J.-P., Langdon, C., & Opdyke, B. N. (1999). Geochemical consequences of increased atmospheric carbon dioxide on coral reefs. *Science*, 284, 118–120. <https://doi.org/10.1126/science.284.5411.118>
- Langdon, C., Broecker, W. S., Hammond, D. E., Glenn, E., Fitzsimmons, K., & Nelson, S. G. (2003). Effect of elevated CO₂ on the community metabolism of an experimental coral reef. *Global Biogeochemical Cycles*, 17(1), 1011. <https://doi.org/10.1029/2002GB001941>
- Lauvset, S. K., Gruber, N., Landschützer, P., Olsen, A., & Tjiputra, J. (2015). Trends and drivers in global surface ocean pH over the past 3 decades. *Biogeosciences*, 12(5), 1285–1298. <https://doi.org/10.5194/bg-12-1285-2015>
- Lewis, E., & Wallace, D. (1998). *Program developed for CO₂ system calculations (ORNL/CDIAC-105)*. Oak Ridge, TN: Carbon Dioxide Information Analysis Center, Oak Ridge National Laboratory, U.S. Department of Energy. <https://www.nodc.noaa.gov/ocads/oceans/CO2SYS/cdiac105.pdf>

- Lueker, T. J., Dickson, A. G., & Keeling, C. D. (2000). Ocean pCO₂ calculated from dissolved inorganic carbon, alkalinity, and equations for K₁ and K₂: Validation based on laboratory measurements of CO₂ in gas and seawater at equilibrium. *Marine Chemistry*, *70*, 105–119. [https://doi.org/10.1016/S0304-4203\(00\)00022-0](https://doi.org/10.1016/S0304-4203(00)00022-0)
- Midorikawa, T., Ishii, M., Saito, S., Sasano, D., Kosugi, N., Motoi, T., et al. (2010). Decreasing pH trend estimated from 25-yr time-series of carbonate parameters in the western North Pacific. *Tellus, Series B*, *62*(5), 649–659. <https://doi.org/10.1111/j.1600-0889.2010.00474.x>
- Millero, F. J., Lee, K., & Roche, M. (1998). Distribution of alkalinity in the surface waters of the major oceans. *Marine Chemistry*, *60*, 111–130. [https://doi.org/10.1016/S0304-4203\(97\)00084-4](https://doi.org/10.1016/S0304-4203(97)00084-4)
- Mucci, A. (1983). The solubility of calcite and aragonite in seawater at various salinities, temperatures, and one atmosphere total pressure. *American Journal of Science*, *283*, 780–799. <https://doi.org/10.2475/ajs.283.7.780>
- Nakano, H., Ishii, M., Rodgers, K. B., Tsujino, H., & Yamanaka, G. (2015). Anthropogenic CO₂ uptake, transport, storage, and dynamical controls in the ocean imposed by the meridional overturning circulation: A modeling study. *Global Biogeochemical Cycles*, *29*, 1706–1724. <https://doi.org/10.1002/2015GB005128>
- Olsen, A., Key, R. M., van Heuven, S., Lauvset, S. K., Velo, A., Lin, X., et al. (2016). The Global Ocean Data Analysis Project version 2 (GLODAPv2)—An internally consistent data product for the world ocean. *Earth System Science Data*, *8*, 297–323. <https://doi.org/10.5194/essd-8-297-2016>
- Olsen, A., Lange, N., Key, R. M., Tanhua, T., Álvarez, M., Becker, S., et al. (2019). GLODAPv2.2019—An update of GLODAPv2. *Earth System Science Data*, *11*, 1437–1461. <https://doi.org/10.5194/essd-11-1437-2019>
- Ono, H., Kosugi, N., Toyama, K., Tsujino, H., Kojima, A., Enyo, K., et al. (2019). Acceleration of ocean acidification in the western North Pacific. *Geophysical Research Letters*, *46*, 13,161–13,169. <https://doi.org/10.1029/2019GL085121>
- Pandolfi, J. M., Connolly, S. R., Marshall, D. J., & Cohen, A. L. (2011). Projecting coral reef futures under global warming and ocean acidification. *Science*, *333*, 418–422. <https://doi.org/10.1126/science.1204794>
- Pfeil, B., Olsen, A., Bakker, D. C. E., Hankin, S., Koyuk, H., Kozyr, A., et al. (2013). A uniform, quality controlled Surface Ocean CO₂ Atlas (SOCAT). *Earth System Science Data*, *5*, 125–143. <https://doi.org/10.5194/essd-5-125-2013>
- Poisson, A., Metzl, N., Brunet, C., Schauer, B., Brés, B., Ruiz-Pino, D., & Louanchi, F. (1993). Variability of sources and sinks of CO₂ and in the western Indian and Southern Oceans during the year 1991. *Journal of Geophysical Research*, *98*, 22,759–22,778. <https://doi.org/10.1029/93JC02501>
- Resplandy, L., Bopp, L., Orr, J. C., & Dunne, J. P. (2013). Role of mode and intermediate waters in the future ocean acidification: Analysis of CMIP5 models. *Geophysical Research Letters*, *40*, 3091–3095. <https://doi.org/10.1002/grl.50414>
- Roberts, C. M., McClean, C. J., Veron, J. E. N., Hawkins, J. P., Allen, G. R., McAllister, D. E., et al. (2002). Marine biodiversity hotspots and conservation priorities for tropical reefs. *Science*, *295*, 1280–1284. <https://doi.org/10.1126/science.1067728>
- Rodgers, K. B., Blanke, B., Madec, G., Aumont, O., Ciais, P., & Dutay, J.-C. (2003). Extratropical sources of equatorial Pacific upwelling in an OGCM. *Geophysical Research Letters*, *30*, 1084. <https://doi.org/10.1029/2002GL016003>
- Sabine, C. L., Feely, R. A., Gruber, N., Key, R. M., Lee, K., Bullister, J. L., et al. (2004). The oceanic sink for anthropogenic CO₂. *Science*, *305*(5682), 367–371. <https://doi.org/10.1126/science.1097403>
- Sabine, C. L., Feely, R. A., Key, R. M., Bullister, J. L., Millero, F. J., Lee, K., et al. (2002). Distribution of anthropogenic CO₂ in the Pacific Ocean. *Global Biogeochemical Cycles*, *16*(4), 1083. <https://doi.org/10.1029/2001GB001639>
- Sabine, C. L., Key, R. M., & Hall, M. (1999). *Carbon Dioxide, hydrographic, and chemical data obtained during the R/V Thomas G. Thompson cruise in the Pacific Ocean (WOCE section P10, October 5–November 10, 1993)* (ORNL/CDIAC-122, NDP-071). Oak Ridge, TN: Carbon Dioxide Information Analysis Center, Oak Ridge National Laboratory, U.S. Department of Energy.
- Schlunegger, S., Rodgers, K. B., Sarmiento, J. L., Frölicher, T. L., Dunne, J., Ishii, M., & Slater, R. (2019). Emergence of anthropogenic signals in the ocean carbon cycle. *Nature Climate Change*, *9*, 719–725. <https://doi.org/10.1038/s41558-019-0553-2>
- Sloyan, B., Johnson, G. C., & Kessler, W. S. (2003). The Pacific cold tongue: A pathway for interhemispheric exchange. *Journal of Physical Oceanography*, *33*, 1027–1043. [https://doi.org/10.1175/1520-0485\(2003\)033<1027:TPCTAP>2.0.CO;2](https://doi.org/10.1175/1520-0485(2003)033<1027:TPCTAP>2.0.CO;2)
- Suzuki, T., Ishii, M., Aoyama, M., Christian, J. R., Enyo, K., Kawano, T., et al. (2013). *PACIFICA data synthesis project* (ORNL/CDIAC-159, NDP-092). Oak Ridge, TN: Carbon Dioxide Information Analysis Center, Oak Ridge National Laboratory, U.S. Department of Energy. https://doi.org/10.3334/CDIAC/OTG.PACIFICA_NDP092
- Takahashi, T., Sutherland, S., Feely, R. A., & Cosca, C. E. (2003). Decadal variation of the surface water PCO₂ in the western and central equatorial Pacific. *Science*, *302*, 852–856. <https://doi.org/10.1126/science.1088570>
- Takahashi, T., Sutherland, S. C., Wanninkhof, R., Sweeney, C., Feely, R. A., Chipman, D. W., et al. (2009). Climatological mean and decadal change in surface ocean pCO₂, and net sea–air CO₂ flux over the global oceans. *Deep Sea Research Part II*, *56*, 554–577. <https://doi.org/10.1016/j.dsr2.2008.12.009>
- Takatani, Y., Enyo, K., Iida, Y., Kojima, A., Nakano, T., Sasano, D., et al. (2014). Relationships between total alkalinity in surface water and sea surface dynamic height in the Pacific Ocean. *Journal of Geophysical Research: Oceans*, *119*, 2806–2814. <https://doi.org/10.1002/2013JC009739>
- Tanhua, T., van Heuven, S., Key, R. M., Velo, A., Olsen, A., & Schirmick, C. (2010). Quality control procedures and methods of the CARINA database. *Earth System Science Data*, *2*, 35–49. <https://doi.org/10.5194/essd-2-35-2010>
- Toyama, K., Rodgers, K. B., Blanke, B., Iudicone, D., Ishii, M., Aumont, O., & Sarmiento, J. L. (2017). Large reemergence of anthropogenic carbon into the ocean's surface mixed layer sustained by the ocean's overturning circulation. *Journal of Climate*, *30*, 8615–8631. <https://doi.org/10.1175/JCLI-D-16-0725.1>
- Wanninkhof, R., & Thoning, K. (1993). Measurement of fugacity of CO₂ in surface water using continuous and discrete sampling methods. *Marine Chemistry*, *44*, 189–204. [https://doi.org/10.1016/0304-4203\(93\)90202-Y](https://doi.org/10.1016/0304-4203(93)90202-Y)
- Weiss, R. F. (1974). Carbon dioxide in water and seawater: The solubility of a non-ideal gas. *Marine Chemistry*, *2*, 23–25. [https://doi.org/10.1016/0304-4203\(74\)90015-2](https://doi.org/10.1016/0304-4203(74)90015-2)
- WMO (2017). WDCGG data summary, 41, <https://gaw.kishou.go.jp/publications/summary>
- Wong, C. S., Chan, Y.-H., Page, J. S., Smith, G. E., & Bellegay, R. D. (1993). Changes in equatorial CO₂ flux and new production estimated from CO₂ and nutrient levels in Pacific surface waters during the 1986/87 El Niño. *Tellus B*, *45*, 64–79. <https://doi.org/10.3402/tellus.v45i1.15580>
- WorldFish (2019). ReefBase: A global information system for coral reefs. *May, 2019*, Retrieved from. http://www.reefbase.org/global_database/
- Zhai, P., Rodgers, K. B., Griffies, S. M., Slater, R. D., Iudicone, D., Sarmiento, J. L., & Resplandy, L. (2017). Mechanistic drivers of anthropogenic carbon in the equatorial Pacific. *Geophysical Research Letters*, *44*, 9433–9439. <https://doi.org/10.1002/2017GL073758>